Research Square

Preprints are preliminary reports that have not undergone peer review.
They should not be considered conclusive, used to inform clinical practice,
or referenced by the media as validated information.

Impact of tephra fallout from the largest explosive basaltic eruption in Iceland: The Veiðivötn 1477 CE eruption (VEI 6)

Léa Guichard

guichard@ipgp.fr

Institut de physique du globe de Paris

Méline Payet--Clerc

Institut de physique du globe de Paris

Guillaume Carazzo

Institut de physique du globe de Paris

Laurie Barrier

Institut de physique du globe de Paris

Research Article

Keywords: Veiðivötn 1477 CE eruption, Tephra dispersal, Fall3D, Copernicus Arctic Regional ReAnalysis, Volcanic hazard assessment

Posted Date: November 26th, 2026

DOI: https://doi.org/10.21203/rs.3.rs-11680314/v1

License: This work is licensed under a Creative Commons Attribution 4.0 International License.
Read Full License

Additional Declarations: No competing interests reported.

Impact of tephra fallout from the largest explosive basaltic eruption in Iceland: The Veiðivötn 1477 CE eruption (VEI 6)

Léa Guichard[1], Méline Payet--Clerc[1,2], Guillaume Carazzo[1], Laurie Barrier[1]

[1]Institut de Physique du Globe de Paris, Université Paris Cité, CNRS, F-75005 Paris, France

[2]Institute of Earth Sciences, University of Iceland, 102, Reykjavik, Iceland

Corresponding author: Léa Guichard, guichard@ipgp.fr

L. Guichard: ORCID 0009-0005-4146-8595

M. Payet--Clerc: ORCID 0009-0000-2089-5081

G. Carazzo: ORCID 0000-0003-0395-2595

L. Barrier: ORCID 0000-0003-3954-8623

Abstract

The Veiðivötn-Bárðarbunga volcanic system has produced several large explosive eruptions, including one of the largest explosive basaltic eruptions ever documented in Iceland. The 1477 CE Plinian eruption injected 10 km^3 of tephra into the stratosphere that mostly deposited on land, covering half of the island with centimeters to meters-thick pumice and ash fallout layers. The widespread dispersion of the deposits raises important questions about the consequences of a similar event occurring today, particularly in terms of tephra fallout hazards. Here, we investigate this issue by modeling the 1477 eruption with the FALL3D numerical model, and confronting it with 30 years of wind data from the Copernicus CARRA reanalysis. Wind analyses allow us to identify two seasonal regimes characterized by contrasting speed

and direction patterns. We performed deterministic simulations to calibrate the eruption source parameters (i.e., plume height and eruption duration) by identifying the combination of volcanological and meteorological inputs that best reproduce the observed 1477 tephra ground load. The best-fit parameters were then used to simulate the 1477 eruption scenario under 1,000 different meteorological conditions using a Monte Carlo approach. These simulations allow us to generate impact maps showing (i) the 5% exceedance probability of different tephra loading thresholds, and (ii) the probability of exceeding four ground-load thresholds (1, 10, 100, and 1,000 kg m^{-2}). Our results highlight the high exposure of critical infrastructure in case of such an eruption. Overall, this study provides a reproducible framework for assessing tephra fallout hazards and supporting volcanic risk preparedness.

Keywords: Veiðivötn 1477 CE eruption, Tephra dispersal, Fall3D, Copernicus Arctic Regional ReAnalysis, Volcanic hazard assessment.

Introduction

Explosive volcanic eruptions may generate Plinian columns that can rise into the atmosphere until reaching a neutral buoyancy height, where they spread laterally forming an umbrella ash cloud (Woods, 1988; Sparks et al., 1997). These eruptions may inject large quantities of volcanic ash into the atmosphere, which can be transported over hundreds to thousands of kilometers (Costa et al., 2013). The maximum extent of tephra dispersal depends on several parameters including eruption magnitude, plume height, grain size distribution, particle density, and atmospheric conditions such as wind speed and direction (Folch, 2012). Atmospheric ash clouds and tephra fallout pose significant hazards to air traffic, human health, agriculture, and infrastructure (Wilson et al., 2012; Jenkins et al., 2015). Consequently, investigating how different physical and environmental parameters influence plume dynamics, cloud spreading, and tephra transport and deposition is essential to better understand dispersal processes and improve volcanic hazard assessment.

Numerous volcanoes have produced sub-Plinian to Plinian eruption columns in recent history, including Vesuvius in 79 CE (Carey and Sigurdsson, 1987), Taupo in 186 CE (Walker, 1980), Mount Saint Helens in 1980 (Carey et al., 1990), Pinatubo in 1991 (Holasek et al., 1996), Chaiten in 2008 (Watt et al., 2009), and Cordon Caulle in 2015 (Bonadonna et al., 2015). These historical eruptions have provided much of our current understanding of Plinian eruption dynamics and tephra dispersal. Although highly explosive eruptions are commonly associated with silicic magmas due to their generally higher volatile contents and viscosities that promote magma fragmentation (Gonnermann and Manga, 2007), basaltic magmas can also produce powerful explosive eruptions. The high explosivity of basaltic magmas is commonly attributed to deep and/or sub-aerial magma water interaction (Wohletz et al., 2013) or rapid decompression in the conduit leading to microlites formation and brittle fragmentation (Moreland et al., 2019). Historical and geological records show that Icelandic volcanoes are prone to explosive basaltic eruptions producing ash clouds and tephra fallout (Thordarson and Höskuldsson, 2008). Among those explosive events, the Veiðivötn 1477 CE eruption stands out as Iceland's largest (magnitude of 6.1) and most powerful (intensity of 11.4) basaltic Plinian eruption of the Holocene (Larsen, 1982; Larsen et al., 2014; Payet--Clerc et al., 2026). Tephra fallout hazards have been assessed for several Icelandic volcanoes through numerical simulations of historical eruptions, including the VEI 6 silicic eruption of Öræfajökull in 1362 CE (Barsotti et al., 2018). However, the impacts of the 1477 CE Veiðivötn basaltic eruption, recently estimated to have reached VEI 6, remain poorly constrained.

The Veiðivötn-Bárðarbunga volcanic system is a discontinuous 60–65 km-long fissure system, composed of multiple segments extending into the Torfajökull central volcano (Larsen et al., 2014). It is one of the most active in Iceland, responsible for some of the island's largest explosive eruptions (Icelandic Meteorological Office). During the Veiðivötn 1477 CE eruption, explosive activity occurred along the entire fissure before gradually transitioning to effusive activity in some places, producing minor lava flows (Larsen, 1984). The eruption produced about 10 km³ of basaltic tephra together with smaller volumes of rhyolitic tephra and lava

(Larsen et al., 2014). Decades of fieldwork have allowed the reconstruction of the stratigraphic sequence and the estimation of several key eruption source parameters (Benjaminsson, 1982; Larsen, 1984, 2005, 2014; Payet--Clerc et al., 2026), including the column height, eruption duration and total grain-size distribution. This VEI 6 eruption is therefore a particularly interesting case-study for testing numerical tephra dispersion models, given its large magnitude and well-preserved deposits distributed across Iceland (Costa et al., 2006; Folch et al., 2009; Barsotti et al., 2018).

Field observations provide quantitative constraints on eruption source parameters (ESPs), which can be used in turn as inputs for numerical tephra dispersal models. However, the extent to which the estimated ESPs can reproduce the observed deposits under different atmospheric conditions remains to be determined. To address this question, we used the FALL3D model (Folch et al., 2009) to simulate tephra transport and deposition under a wide range of meteorological conditions. Model outputs were compared with field observations to identify the eruptive scenario that best reproduces the mapped deposits. By repeatedly simulating the same eruption under different atmospheric scenarios, FALL3D provides a framework for investigating the influence of wind variability on tephra dispersal and generating probabilistic hazard maps. Thus, we used the calibrated eruption source parameters of the Veiðivötn 1477 CE eruption to perform 1,000 Monte Carlo simulations spanning 30 years of meteorological conditions (1994–2024) in order to characterize the variability in tephra dispersal associated with changing wind conditions. Following the probabilistic framework of previous studies (Folch and Sulpizio, 2010; Bonasia et al., 2011; Barsotti et al., 2018; Michaud-Dubuy et al., 2021, 2024, 2025), we combined the resulting simulations to generate probabilistic hazard maps showing the likelihood of exceeding selected tephra accumulation thresholds across Iceland.

The resulting probabilistic hazard maps provide an effective tool for identifying areas exposed to tephra fallout and informing stakeholders involved in mitigation planning and risk communication, by highlighting vulnerable regions and critical infrastructures such as roads,

power stations, and airports (Loughlin et al., 2017; Barsotti et al., 2018; Michaud-Dubuy et al., 2025). By evaluating the impacts of a large VEI 6 eruption under current atmospheric conditions, our study contributes to ongoing efforts aimed at improving volcanic risk preparedness in Iceland, and supports the development of hazard mitigation strategies.

2. **Materials and Methods**

The methodology adopted in this study is structured around four main steps, combining both deterministic and probabilistic approaches. The deterministic approach aims to numerically reproduce the observed tephra ground loads in the field associated with the Veiðivötn 1477 CE eruption. This first step involves (i) determining the most suitable eruption source parameters such as column height, eruption duration and total grain size distribution, and (ii) identifying the meteorological conditions in the wind database that best reproduce the observed deposits pattern. In the probabilistic framework, the eruption source parameters derived from the deterministic calculations are combined with the 30-year meteorological dataset to (iii) produce three composite hazard maps corresponding to the 5% exceedance probability depending on the months of the year taken into account, and (iv) generate hazard maps representing the probability of exceeding four thresholds of tephra ground loads (1, 10, 100 and 1,000 kg/m²), each associated to different severity of damages. The 5% probability of exceedance maps illustrate the tephra load reached in 5% of the simulations, providing an integrated overview of potential fallout across the dataset and includes key infrastructures and towns likely to be impacted by a future eruption of similar magnitude.

2.1 **Geological dataset**

Defining an eruptive scenario requires the integration of geological constraints derived from field observations. To this end, we compiled 288 georeferenced field observations made by Benjaminsson (1982), Larsen (1984), and Payet--Clerc et al. (2026). These observations include detailed information on outcrop location (Figure 1 and Table S1), tephra thickness and/or ground load, as well as grain size distributions (Figure 2 and Table S2). We used the

resulting dataset as reference points to evaluate the reliability and accuracy of our numerical simulations. Note that medial outcrops are missing in field-based studies because of restricted access and poor preservation of the deposit due the presence of the Vatnajökull ice cap.

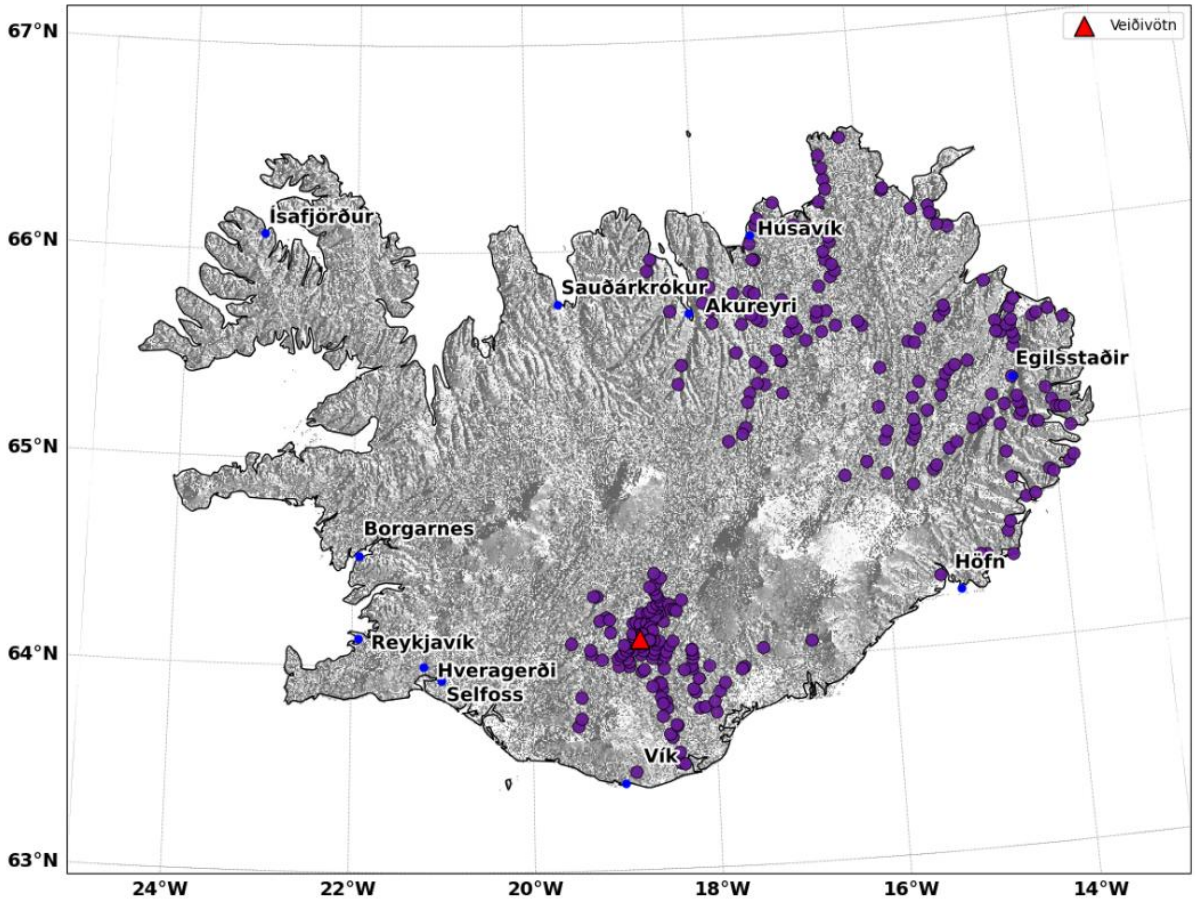

Figure 1: Map of Iceland showing the location of the Veiðivötn volcanic fissure (red triangle), the main cities (blue squares), and the outcrops used in this study (purple circles) from Benjaminsson (1982), Larsen (1984), and Payet--Clerc et al. (2026). All the maps presented in this paper are displayed in the UTM Zone 27N projection. GPS coordinates and ground load measurements are available in Table S1.

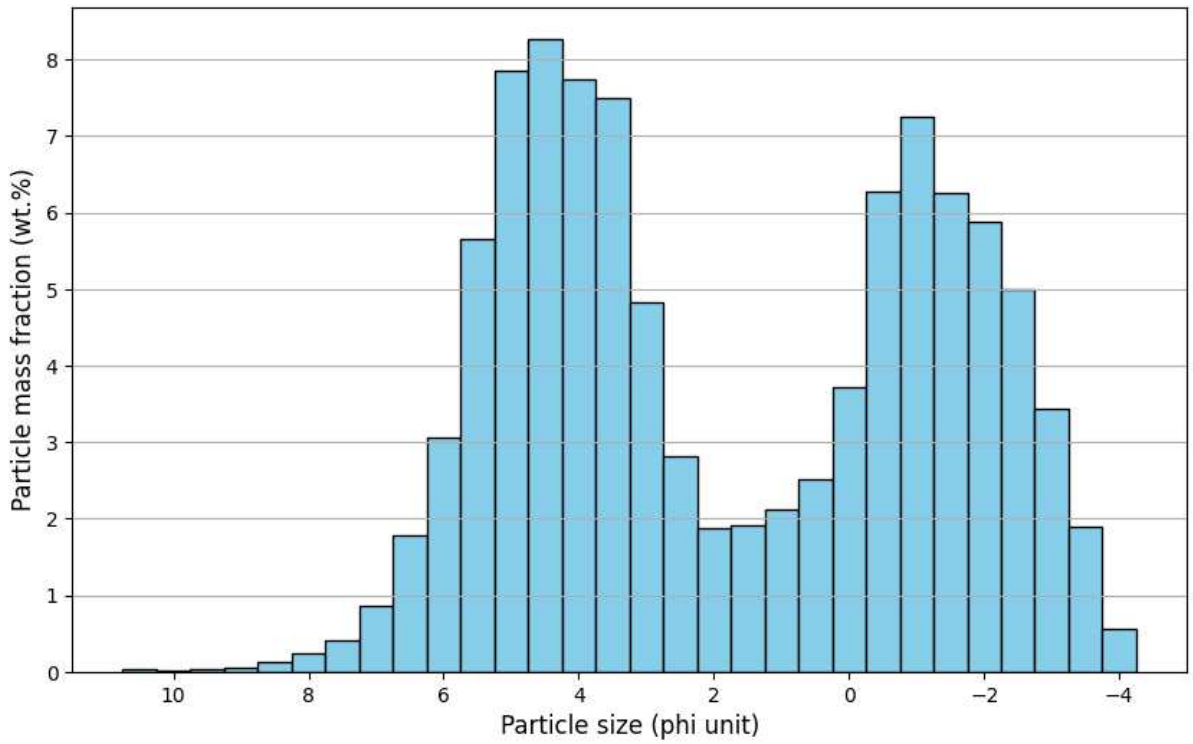

Figure 2: Total grain size distribution of the 1477 CE Veiðivötn eruption used in all the simulations (Payet--Clerc et al., 2026). Particle mass fraction, density and sphericity are available for each size class in Table S2.

2.2 **Meteorological dataset**

We used the CARRA1 dataset (Copernicus Arctic Regional ReAnalysis; Schyberg et al., 2020) to provide the atmospheric forcing for our dispersal simulations. This dataset is made available by the Copernicus Climate Change Service (C3S) through the Copernicus Climate Data Store (CDS). CARRA is a regional reanalysis driven by boundary conditions from ECMWF's fifth-generation global atmospheric reanalysis (ERA5), providing meteorological data at a horizontal resolution of 2.5 km, on 23 pressure levels ranging from 1,000 to 10 hPa, and at a temporal resolution of 3 hours. The CARRA-East database covers our area of interest spanning 25–13°W and 63–67°N as it focuses on the eastern European sector of the Arctic. We retrieved the meteorological data from the Copernicus Climate Data Store (CDS) on a regular 1° × 1° latitude–longitude grid using linear interpolation, at 12-hour intervals, from

January 1, 1994 (00:00 UTC) to December 31, 2024. This preprocessing preserves the large-scale circulation patterns (Figure S1) that control the transport of volcanic ash. Our final dataset is thus composed of 22 646 vertical wind profiles.

As wind conditions strongly control tephra dispersal (Lacasse, 2001; Larsen et al., 2014), the CARRA dataset was further analysed to identify distinct seasonal wind regimes and account for them in the dispersal simulations. A marked seasonality of atmospheric circulation over Iceland due to seasonal changes in North Atlantic atmospheric circulation has been considered in previous volcanic-hazard assessments, in which season-dependent meteorological conditions were used to account for changes in tephra dispersal patterns (Lacasse, 2001; Barsotti et al., 2018). Stratospheric winds are expected to exert the primary control on tephra transported by Plinian eruption columns, however, previous studies showed that tropospheric winds can also influence the plume evolution and ash deposition (Michaud-Dubuy et al., 2021). Thus, both atmospheric layers were analysed to characterize the seasonal wind regimes over Iceland and identify meteorological wind conditions for the dispersal simulations (Figures 3, 4 and S1). The frequency of winds coming from each direction and associated wind-speed classes are represented via wind roses, constructed using CARRA wind data between 1,000 hPa and 10 hPa, from 1994 to 2024, considering observations at 00:00 and 12:00 UTC (Figure 3a and 3b).

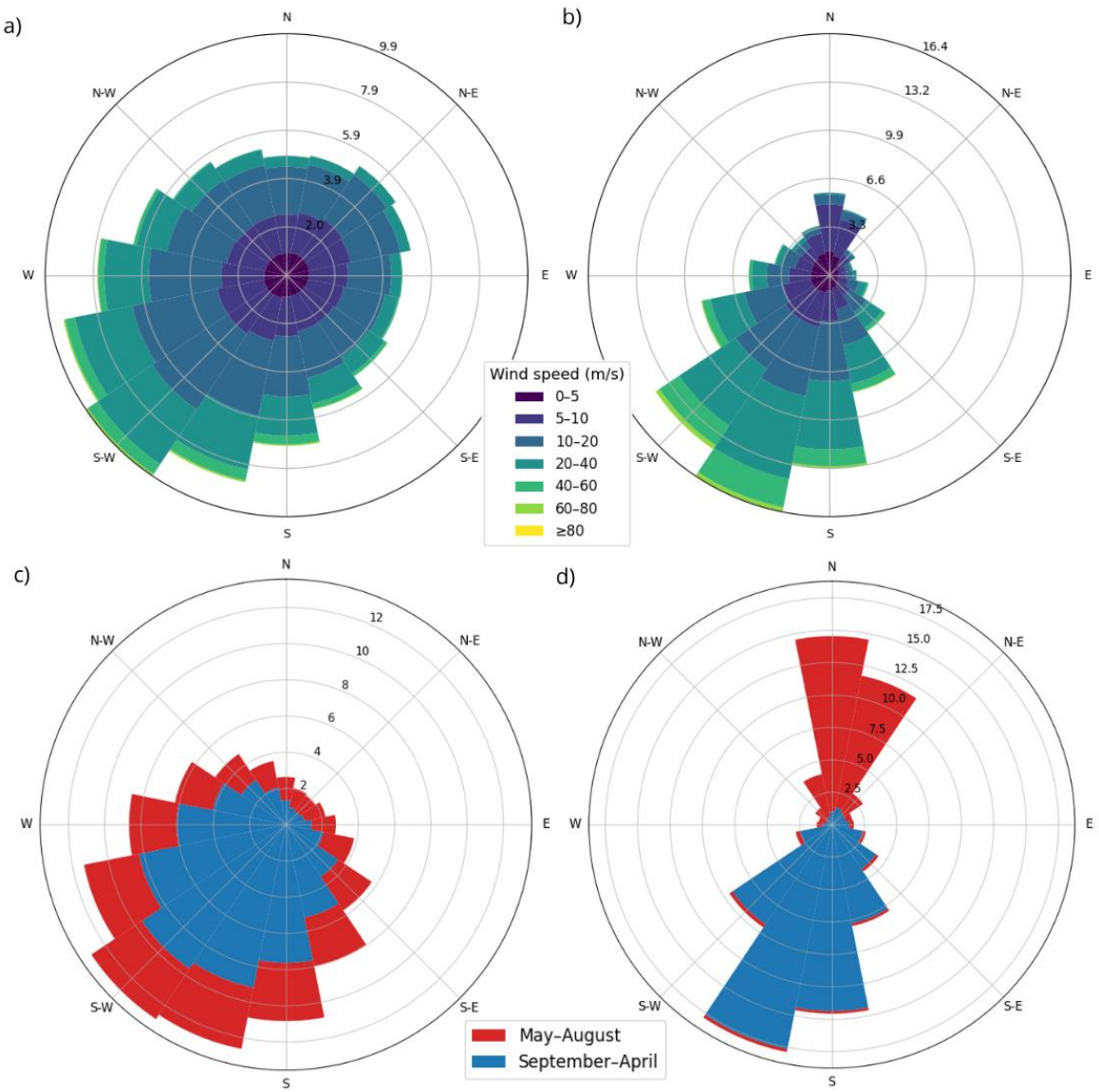

168

169 **Figure 3.** Wind roses derived from 30 years of ECMWF data (1994–2024) and spatially
170 averaged over Iceland. (a) Tropospheric winds between 1,000 and 300 hPa and (b)
171 stratospheric winds between 250 and 10 hPa, showing wind speed and direction. Seasonal
172 wind-direction frequencies are shown at (c) 250 hPa and (d) 10 hPa for summer (May–August,
173 in red) and winter (September–April, in blue). Wind roses indicate the direction from which the
174 wind blows. Petal length represents the frequency of winds originating from each direction.

175

176 2.3 **Eruption source parameters**

The FALL3D dispersal model requires as input the maximum column height, the eruption duration, and the total grain size distribution (TGSD), including particle density and sphericity (Costa et al., 2006; Folch et al., 2009; Folch, 2012). The column height controls the altitude at which particles are injected into the atmosphere and transported by the wind, whereas the eruption duration determines the total mass of particles released into the eruption column. Both parameters can be constrained from field studies using the deposit characteristics such as grain size distributions and deposit thicknesses. A recent field study gives a column height of 30 ± 3 km and a duration of 12.3 ± 4 hours (Payet--Clerc et al., 2026). We thus varied the column height from 8 to 40 km, and the eruption duration from 5 to 20 h in order to account for possible large uncertainties in the field-based estimates. The TGSD used in all our calculations (Figure 2) was determined from grain size measurements at each outcrop (Payet--Clerc et al., 2026). Particle density and sphericity distributions (Table S2) were determined from laboratory measurements together with the model of Kaminski and Jaupart (1998).

2.4 **Determination of the best-fit simulation**

We first performed a series of single scenario simulations based on the eruption source parameters retrieved for the Veiðivötn 1477 CE eruption. We built a composite scoring framework combining four complementary performance metrics in order to select the best-fitting volcanological and meteorological conditions (Table 1). The most influential metric F5 measures the proportion of simulated deposits values falling within a factor of five of the observed values. This type of factor-based indicator quantifies the overall agreement between model and field data, and is widely used in atmospheric dispersion model evaluation (Chang & Hanna, 2004; Bonadonna et al., 2005). We also considered the logarithmic root mean square error (logRMSE), which quantifies the average multiplicative distance between simulated and observed values. This metric gives greater weight to large mismatches and thus distinguishes runs with similar F5 values but different levels of extreme error. To evaluate the systematic over- or underestimation of the simulations, we also used the median multiplicative factor, which measures the systematic bias of the model independently of

204 random scatter and is robust to outliers (Moriasi et al., 2007). Finally, we considered the slope
205 of the log-log linear regression, which assesses the model's ability to reproduce the shape of
206 the deposit gradient. These four metrics were combined together in order to define a global
207 score. To maximize the fit between the modelled tephra deposits and the observations, we
208 assigned a higher weight to F5 (40%), which reflects the proportion of acceptable predictions,
209 and reduced the weight of the slope of the log-log linear regression (10%) since it may be
210 influenced by very proximal and distal deposits that are relatively poorly constrained in the
211 field. This led to weights of 40% to F5, 25% to logRSME, 25% to the median multiplicative
212 factor, and 10% to the slope of the log-log linear regression (Table 1).

213 **Table 1:** Composite scoring framework designed in this study.

Metric	**Evaluation**	**Optimal value**	**Weight**
F5	Fraction of observation reproduced within a factor of 5	1	40%
LogRMSE	Average prediction error	0	25%
Median factor	Systematic over-/underestimation	1	25%
Regression slope	Reproduction of deposit gradient	1	10%

214

215 2.5 **Exploration of the wind effects via Monte Carlo simulations**

216 Exploring a range of meteorological conditions allows the probabilistic assessment of volcanic
217 impacts. To this end, we adopted a Monte Carlo approach in which the eruption source
218 parameters inferred for the 1477 event (Table 2) were kept constant, while we varied the wind

conditions for each simulation in order to generate an ensemble dataset (see also Cioni et al., 2003; Hurst and Smith, 2004; Bonadonna et al., 2005; Macedonio et al., 2008; Costa et al., 2009; Barsotti et al., 2010; Scaini et al., 2012, 2014; Scollo et al., 2013; Biass et al., 2014; Bonasia et al., 2014; Barsotti et al., 2018). In total, we performed 1,000 simulations using wind conditions randomly selected from the 30-year CARRA1 meteorological database (see Section 2.2). This large number of runs allowed us to generate an ensemble of tephra dispersal scenarios from which we derived probabilistic hazard maps.

Table 2: Volcanological input parameters used in this study.

Parameter	**Value**	**Reference**
Plume height	30 km	Payet- -Clerc et al. (2026)
Duration	12 h	Payet- -Clerc et al. (2026)
Tephra mass	1.1 x 10^{13} kg	Payet- -Clerc et al. (2026)
Erupted volume	10 km^3	Larsen (1984), Payet- -Clerc et al. (2026)

2.6 **Impacts of tephra on infrastructures**

Tephra fallout can have a wide range of impacts on populations and infrastructure located near volcanoes. Even relatively thin ash deposits may disrupt daily activities and isolate significant parts of the population by making roads impassable and limiting access to essential services. Critical infrastructure, including electricity production from geothermal and hydroelectric power plants and water supply systems can also be affected through ash contamination, clogging, or damage to distribution networks (Wilson et al., 2012; Jenkins et al., 2015; Blake et al., 2017, Deligne, 2017). To quantify the potential impacts of a future

tephra-producing eruption, we adopted a set of threshold values representative of increasing levels of disruption to infrastructure, services, and daily activities (Table 3; see also Wilson et al., 2012; Jenkins et al., 2015; Michaud-Dubuy et al., 2025).

Table 3: Damages associated with tephra load thresholds used in this study.

Mass load (kg m^{-2})	**Thickness (cm)**	**Damage**	**Reference**
1-10	0.1-1	Reduced road visibility and grip; air traffic disruption; possible clogging and abrasion of power infrastructure; minor clean-up required.	Guffanti et al. (2010), Wilson et al. (2012), Jenkins et al. (2015).
10-100	1-10	Extensive repair on supply networks, possible considerable production losses from impacts on crops and livestock; possible damage to vulnerable roofs; disruption of water and wastewater treatment systems.	Wilson et al. (2012), Jenkins et al. (2015).

100-1,000	10-100	Replacement of severely damaged supply networks; structural damage and possible collapse of vulnerable buildings; possible casualties; prolonged or permanent relocation; chronic respiratory and psychological effects; prolonged economic disruption and associated losses.	Spence et al. (2005), Jenkins et al. (2015).
>1,000	>100	Complete destruction, including major building collapse and possible casualties; total burial of crops and pastures, potentially requiring land-use change;	Spence et al. (2005), Jenkins et al. (2015).

		long-term decline in soil fertility.	

240

241 3. **Results**

242 3.1 - **Seasonal trends**

243 Figures 3 and 4 show our analyses of the meteorological conditions over Iceland using the
244 CARRA dataset. Although markedly different wind regimes are observed between different
245 pressure levels and dates, the wind patterns remain spatially coherent across the study area
246 (Figure S1) allowing us to use spatially averaged conditions over the study area (25–13°W,
247 63–67°N — see Figures 3 and 4). The tropospheric wind rose (Figure 3a) shows significant
248 directional variability, with prevailing southwesterly winds, as indicated by the longer and more
249 frequent petals in the southwest sector (approximately N210–240°). In contrast, the
250 stratospheric wind rose (Figure 3b) shows less directional variability and is dominated by
251 southwesterly winds (approximately N200–220°). Meteorological daily patterns were then
252 obtained by averaging each calendar day across the 30-year dataset (Figure 4). The resulting
253 meteorology reveals a pronounced seasonal variability in both wind speed and direction
254 (Figures 3c, 3d and 4). Two main characteristic periods can be distinguished: a winter regime
255 extending approximately from September to March, and a summer regime from May to July.

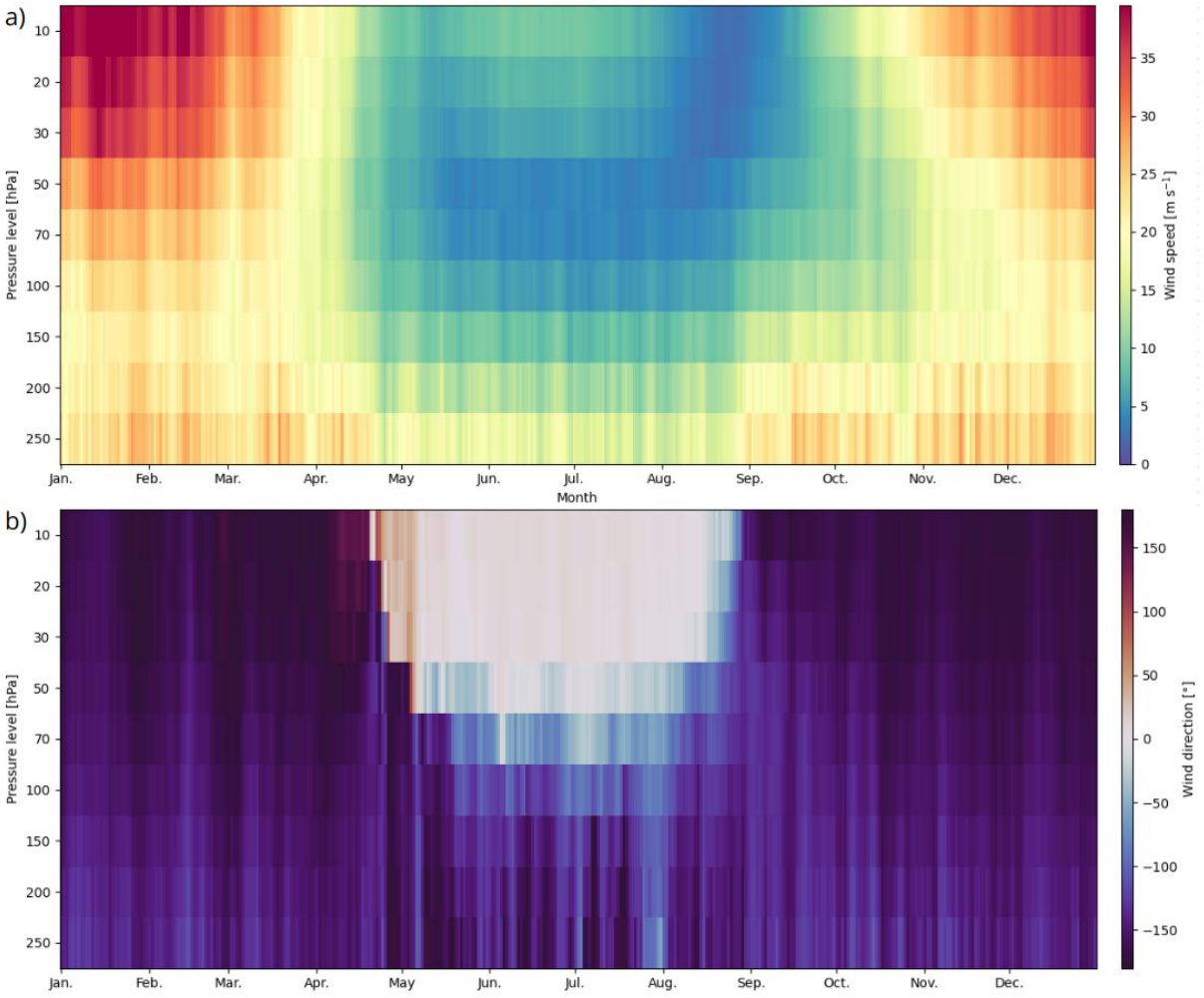

Figure 4: Climatological daily patterns showing 30 years of ECMWF data (1994-2024): (a) wind speed and (b) wind direction as a function of time of year and pressure level (250–10 hPa). Wind speed is expressed in m s^{-1} and wind direction in degrees.

Seasonality is most pronounced at high altitudes (Figure 3d), whereas lower-altitude circulation remains comparatively stable throughout the year, particularly in terms of wind direction (Figure 4). At low levels, winds come predominantly from the southwest, implying transport of tephra towards the northeast during most of the year. A similar southwesterly regime is also observed at high altitudes during winter. However, the seasonal contrast becomes much stronger in altitude during the summer, when this prevailing southwesterly circulation is disrupted by a marked increase in northerly winds. In terms of wind speed, seasonal variability is also less pronounced at low altitudes, although a clear contrast remains,

with stronger winds in winter (20 to 25 m s^{-1}) and weaker winds in summer (10 to 15 m s^{-1}). This difference becomes much more pronounced at high altitudes since summer values generally fall within a range from less than 5 to around 15 m s^{-1}, whereas winter mean values typically range from approximately 20 to more than 35 m s^{-1}.

These pronounced seasonal changes in the vertical wind field are expected to exert a first-order control on the transport and dispersal of volcanic particles. Consequently, an eruption occurring under winter conditions may generate substantially different tephra dispersal patterns from an otherwise comparable eruption occurring during summer.

3.2 - **Single scenario simulations**

The mapped distribution of the 1477 tephra deposits shows that most of the eruptive products were deposited northeast of the vent (Figure 1), indicating that the eruption occurred under predominantly southwesterly winds. The analysis of 30 years of meteorological data revealed that winter conditions best reproduce this dispersal pattern (Figures 3 and 4). We therefore focused our calculations on winter conditions (i.e., January–April and September–December 2024), and simulated the eruption using all available meteorological conditions within these periods (i.e., 213 dates). The resulting FALL3D simulations were then compared with field observations using the composite score detailed in section 2.4 in order to identify the meteorological conditions that best reproduce the observed 1477 deposits.

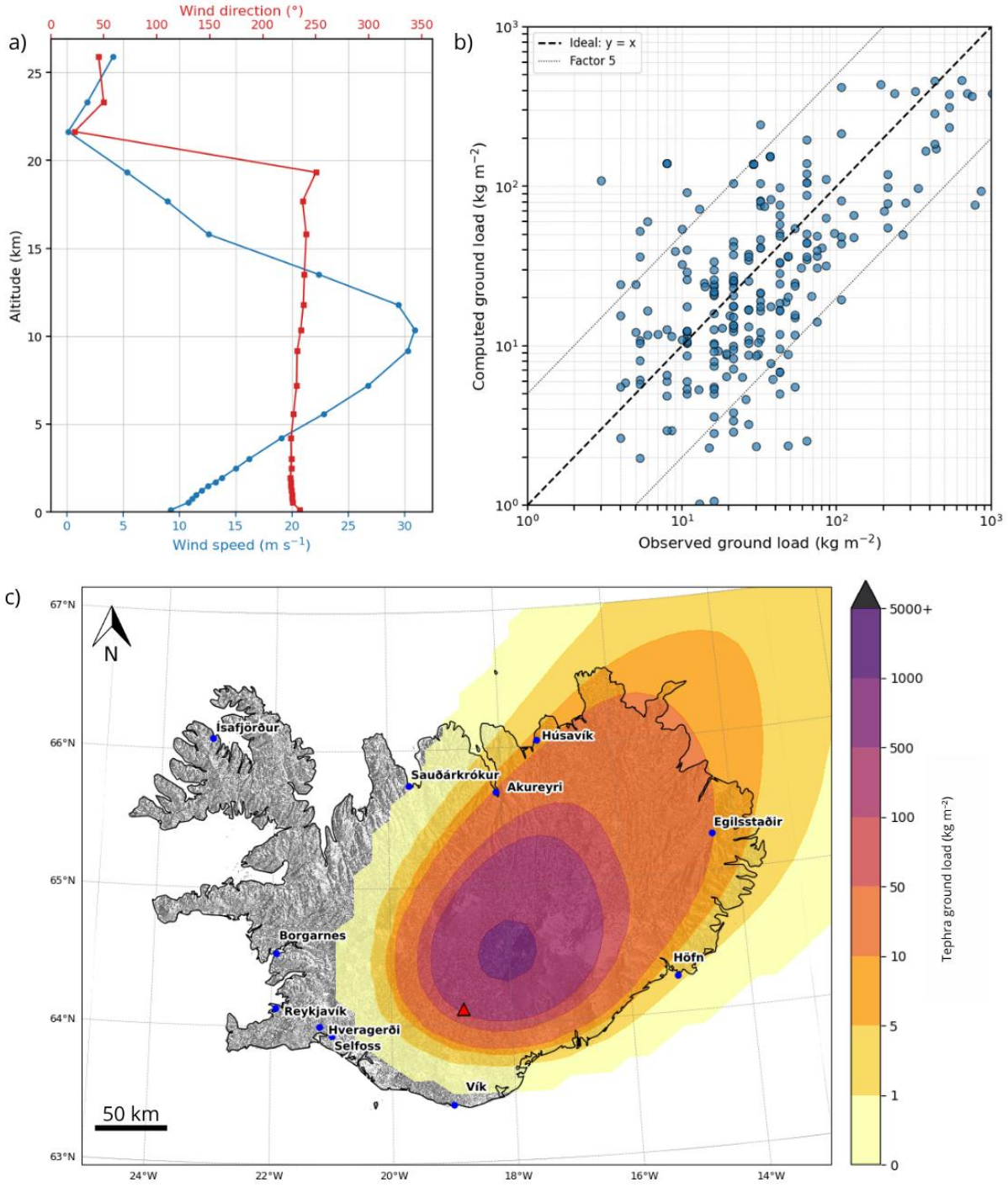

286

287 **Figure 5**: Single-scenario simulation showing the best-fit to reproduce the Veiðivötn 1477 CE
288 eruption: a) wind speed and direction profiles, b) computed versus measured ground loads,
289 and c) deterministic map. The map is displayed in the UTM Zone 27N projection.

290 Among all tested meteorological and volcanological conditions (see section 2.4), the
291 best fit simulation was obtained for a column height of 30 km and an eruption duration of 12

h, in agreement with the results of Payet–Clerc et al. (2026) (column height of 30 ± 3 km and a duration of 12.3 ± 4 hours) and wind speed and direction of 6 September 2024 (composite score of 0.71; Table 4). The wind profile of this specific date is characterized by high wind speeds and limited directional variability (Figure 5a). The resulting log–log comparison shows good agreement between observed and simulated tephra ground loads (Figure 5b). The lack of medial outcrops identified in previous field studies (Figure 1) does not significantly affect our results as the range of computed and observed ground loads continuously covers three orders of magnitude. Figure 5c shows the spatial distribution of the simulated tephra ground load (kg m^{-2}), which reproduces the northeastward dispersal observed for the 1477 deposit (Payet--Clerc et al., 2026). The good agreement between the simulated map under realistic winter meteorological conditions based on the reconstructed eruption parameters and the observed 1477 tephra deposit supports the selected eruption scenario. Having established how such an eruption could behave under winter conditions, we now extend the analysis to a broader range of meteorological scenarios in order to investigate how tephra dispersal and its potential impacts may vary under different atmospheric conditions. To achieve this goal, we used a Monte Carlo approach to assess the likelihood of exceeding different tephra ground-load thresholds across the study area and the associated impacts on populations and infrastructure.

Table 4: Metrics and score corresponding to the best-fit simulation of the 1477 CE Veiðivötn eruption.

Plume height	Duration	F5	logRMSE	Median factor	Regression slope	Total score
30 km	12 h	0.75	0.69	0.69	0.43	0.71

3.3 - **Probabilistic threshold exceedance maps**

The 1,000 FALL3D simulations performed using a Monte Carlo approach (see section 2.5) were used to generate probabilistic hazard maps. To account for seasonal variability in tephra dispersal, we built two seasonal probabilistic maps showing the areas with a 5% probability of exceeding different tephra loading thresholds associated with increasing levels of infrastructure impact. This probability level was selected because it is commonly considered in probabilistic tephra hazard assessments and has been used to support civil protection strategies, particularly in the Lesser Antilles (Michaud-Dubuy et al., 2021, 2025). The winter map is based on 1,000 simulations randomly sampled from meteorological conditions between September 2 and April 30, while the summer map is based on 1,000 simulations sampled between May 1 and September 1 over the 1994–2024 period. Figure 6 shows the resulting maps, which reveal markedly different dispersal patterns between the two seasons. Winter is characterized by preferential northeastward dispersal, associated with stronger winds (Figure 6a). Towns located offshore on the northeastern coast have thus a 5% probability of exceeding relatively high loads (up to 10-50 kg m^{-2} in Husavik and Egilstaddir), whereas towns in the Reykjavik area are likely to experience much lower loads (0-1 kg m^{-2}). In contrast, Summer wind conditions give a more centered distribution of tephra deposits around the source, with no clear preferential dispersal direction, consistent with weaker and more variable winds (Figure 6b). During this season, the city of Reykjavik has a 5% probability of exceeding up to 10-50 kg m^{-2}. Figure 6c combines all the simulations and provides a single hazard map that accounts for the complete wind database. The winter northeastern trend is present but damped by summer winds.

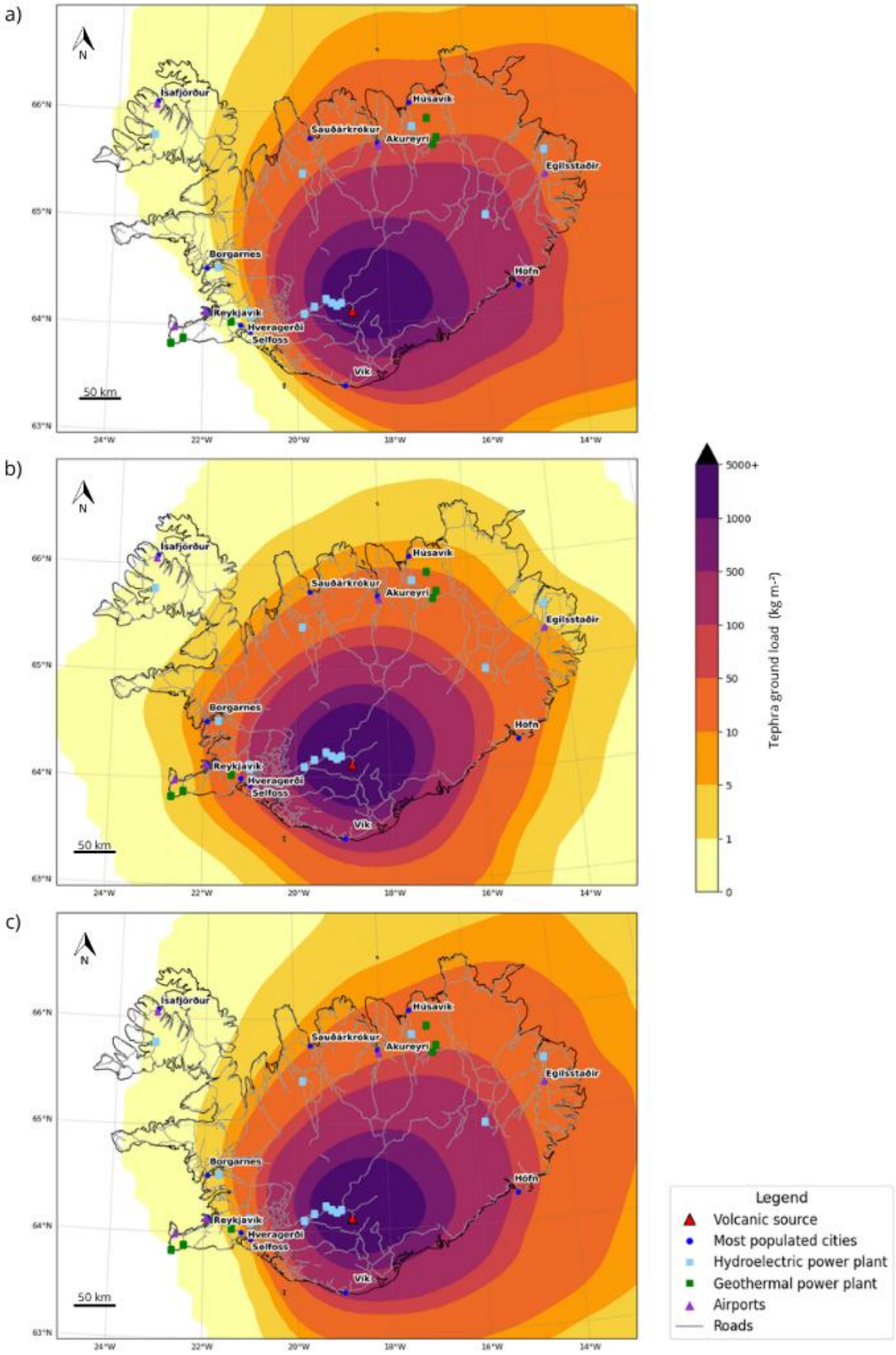

335 **Figure 6:** 5% probabilistic tephra-fall contours based on the 30-year wind dataset for (a) the

winter period and (b) the summer period, as defined from the seasonal wind patterns identified in Figure 4, and (c) the entire year using the complete wind dataset. The maps are displayed in the UTM Zone 27N projection.

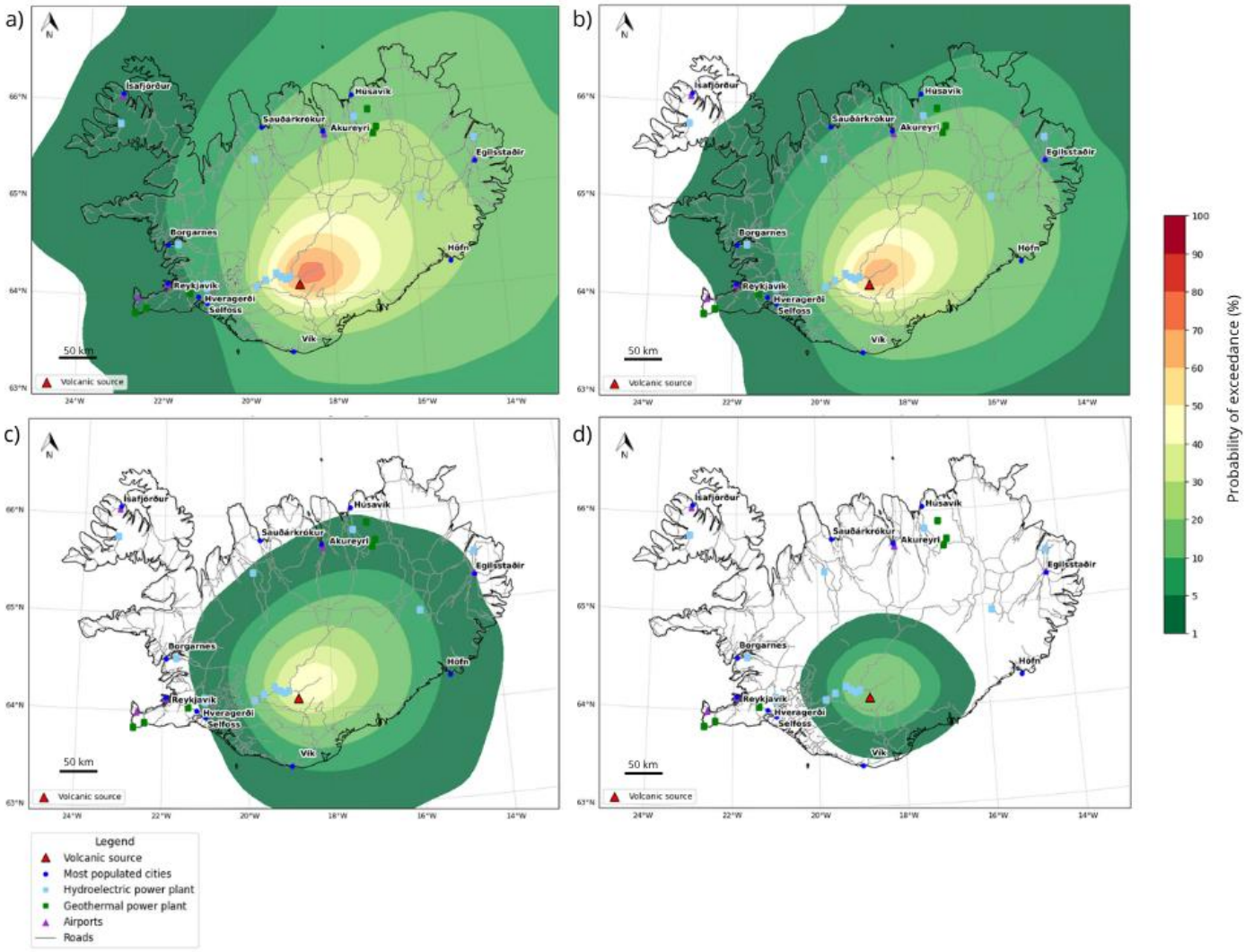

Figure 7: Probabilistic hazard map for tephra loading higher than a) 1, b) 10, c), 100, and d) 1,000 kg m^{-2} using the 30-year wind database. The maps are displayed in the UTM Zone 27N projection.

Figure 7 shows the probability of exceeding 1.0, 10, 100 and 1,000 kg m^{-2} of tephra load with the eruptive parameters of the 1477 eruption under a realistic range of wind conditions over the 1994–2024 period. These thresholds were chosen according to the different scales of the impact associated with each load as described in Table 3. All the maps depict a general northeastward trend, reflecting the meteorological conditions (Figure 3). The

maps also confirm that the lower the threshold investigated, the wider the area of susceptibility, consistent with the thinning of the deposits with distance from the source (Barsotti et al., 2018). Our simulations show that the entire island has a probability of at least 1% to reach a tephra load of 1 kg m^{-2} (Figure 7a), and most of the island has a likelihood of exceeding 10 kg m^{-2}, except on the northwestern peninsula (Figure 7b). The areas impacted by larger thresholds are more restricted. Most towns are not expected to be impacted by a tephra load of 100 kg m^{-2}, except of few localities where the probability of exceeding this threshold reaches 1% (e.g., Egilsstaðir, Selfoss), 1-5% (Höfn, Akureyri), and 5% (Vík) (Figure 7c). The tephra load of 1,000 kg m^{-2} is not expected to affect the main towns, but could impact local communities and power plant infrastructures (Figure 7d).

3.4. **Impact on critical infrastructure**

Tephra ground load thresholds are associated with different levels and types of potential damage (Table 3) and their exceedance probabilities provide a direct indication of the likelihood that infrastructure within a given area will be exposed to potentially damaging tephra loads. At the national scale, the potential impacts are closely related to the spatial distribution of critical infrastructure and transport networks. Heavy tephra fallout could affect several parts of Iceland within only a few hours after eruption onset, leaving limited time for emergency response and protective measures. Depending on wind conditions, substantial tephra accumulation could affect inhabited areas, transport corridors, power networks, water supplies, and other critical infrastructure causing severe disruption in urban centres located downwind through reduced visibility, contamination of water systems, damage to machinery, road closures, and interruption of daily activities (Wilson et al., 2012; Scaini et al., 2014; Barsotti et al., 2018). Livestock farming and exposed ecosystems would also likely be affected over broad areas (Thorvaldsdóttir and Sigbjörnsson, 2015; Jenkins et al., 2015). Overall, such an event could lead to major disruption of essential services and national-scale functioning.

Figures 6 and 7 show that Vík and Höfn are the only towns directly exposed to relatively high tephra loads (>50 kg m^{-2}). Although relatively small in populations (730 inhabitants in Vik and 1,807 in Höfn in 2025 according to Statistics Iceland, 2025), these towns play an important role as service and refuelling hubs for travellers along Iceland's road network. Their disruption could therefore have consequences extending well beyond the number of residents directly affected but rather impact the road transportation at national scale, making travel between different parts of the island difficult. Although the area surrounding the vent is sparsely populated, hydroelectric power plants located near the eruptive source have a 5% probability of being exposed to tephra loads ranging from 100 to over 5,000 kg m^{-2}. Such loads could severely disrupt electricity production and supply, as these facilities are particularly vulnerable. Numerous other towns and geothermal power plants are located in areas where tephra loads corresponding to a 5% exceedance probability range from 10 to 50 kg m^{-2}. Such loads are associated with major disruptions of water supply, electricity networks and roads (Table 3), especially Route 1 in the southern coast (the Ring Road). The international airport of Keflavík, and the domestic airport of Egilsstaðir, also have a 5% probability of exceeding these thresholds, causing long term closure because of the burial of the equipment.

Societal functioning can also be significantly disrupted by low tephra loads (1–10 kg m^{-2}). A ground load of 1 kg m^{-2} is associated with significant disruptions of road networks and air traffic, and a significant increase in health issues (Table 3). Tephra ground loads <1 kg m^{-2} can also disrupt air traffic, as expected for the three airports Reykjavík, Ísafjörður, and Akureyri. The economic consequences could thus extend beyond the areas directly impacted by tephra fallout (Scaini et al., 2014) affecting tourism activities, which represent an important component of the Icelandic economy (8.7% of GDP according to Tourism Satellite Accounts, Statistics Iceland, 2025). The combination of direct tephra impacts and disruption of transportation networks illustrates how a large explosive eruption could generate cascading consequences extending well beyond the areas receiving the highest ash loads.

4. Discussion

Our study highlights that an eruption comparable to the Veiðivötn 1477 CE event would represent a major multi-scale hazard, with impacts extending far beyond the immediate vicinity of the source. The probabilistic simulations show that under some meteorological configurations, tephra dispersal could affect large parts of Iceland. Such basaltic explosive eruptions should therefore not be considered solely in terms of local hazards, but as events capable of producing impacts at the national and possibly much larger scale.

4.1 - **Distal tephra dispersal and regional implications**

The reconstructed maximum plume height of 30 km indicates that the eruption reached the stratosphere, allowing fine ash particles to be transported far beyond Iceland. Such long-range dispersal would pose a major challenge to aviation, as illustrated by the widespread disruption caused by the 2010 Eyjafjallajökull eruption despite its much lower plume height of approximately 9 km, which stands below the stratosphere (Gudmundsson et al., 2010). An eruption similar to the Veiðivötn 1477 event could therefore lead to closures or rerouting of major air corridors between Europe and North America with substantial economic and logistical consequences. Geological observations support this potential widespread dispersion as fine-grained products attributed to the 1477 CE eruption have been identified as distal cryptotephra in Ireland (Chambers et al., 2004), Sweden (Davies et al., 2007), and Greenland (Abbott et al., 2021) (Figure 8). Although these deposits represent very low concentrations of fine particles rather than substantial ash accumulation, they provide direct evidence that the atmospheric footprint of the 1477 eruption extended over thousands of kilometers beyond Iceland. However, despite this extensive dispersal, the eruption likely had a limited climatic impact due to the relatively low altitude of SO_2 injection (Payet, 2026).

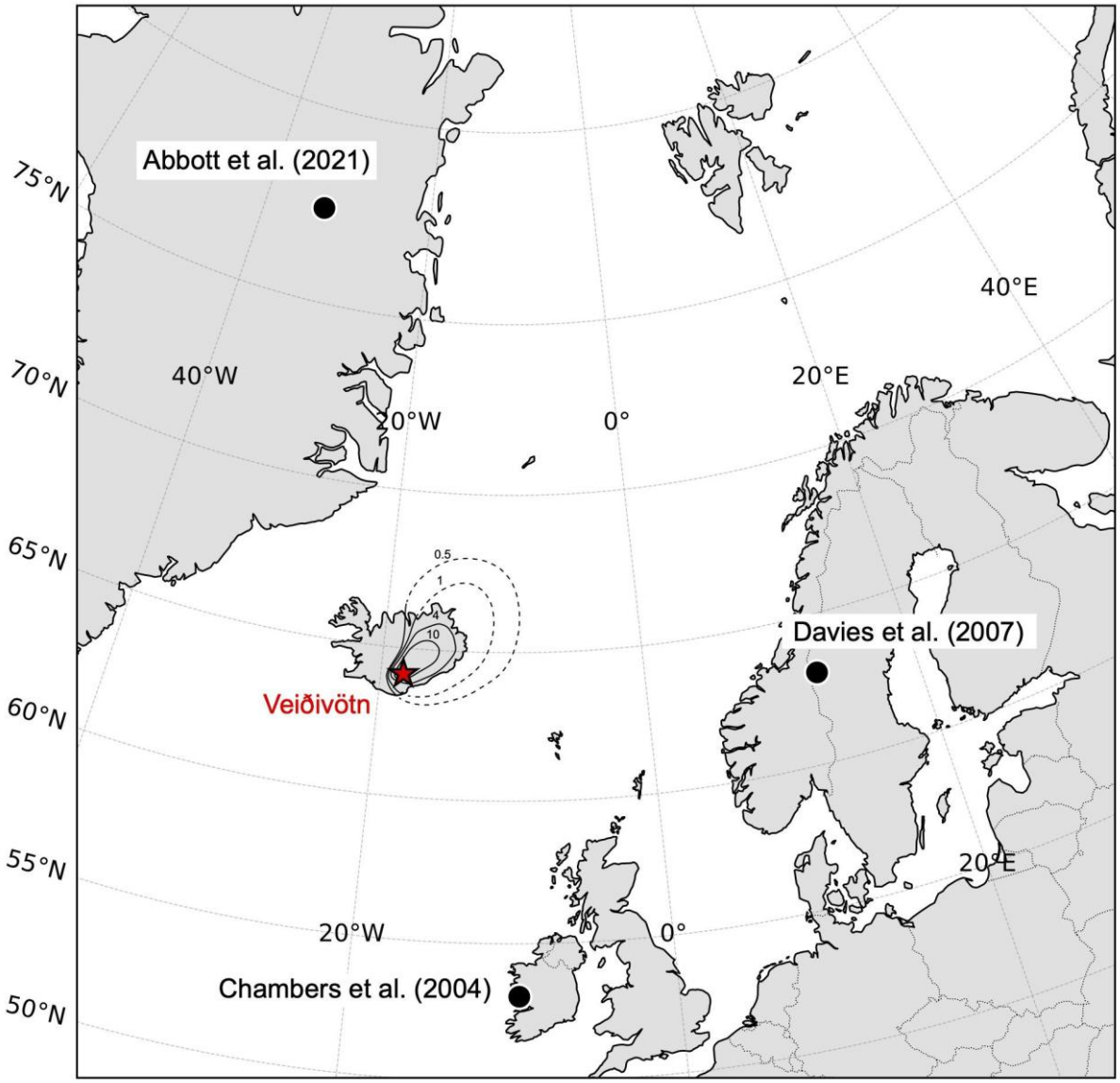

Figure 8: Tephra fall deposit thickness map (in cm) of the 1477 CE Veiðivötn eruption (Payet--Clerc et al., 2026) showing sites where cryptotephra attributed to the eruption have been identified (Chambers et al., 2004; Davies et al., 2007; Abbott et al., 2021).

The potential impacts of such an eruption mainly depend on the maximum plume height but also on the vertical structure of the atmosphere is also important. For instance, strong stratospheric easterly winds capable of transporting fine ash towards the Reykjavík area may be partly counteracted by strong tropospheric westerly winds, thereby limiting ground deposition to the west of the volcano (Figure S2). Consequently, transport at high altitude does not necessarily translate directly into substantial ground deposition, highlighting

the importance of considering the full vertical wind profile when assessing potential tephra impacts. These findings are particularly relevant in the context of present-day volcanic risk management. Renewed volcanic unrest on the Reykjanes Peninsula since 2021 and repeated eruptions near Grindavík between 2023 and 2024, have further emphasized the need for continuous monitoring and regularly updated hazard assessments, including in regions that had experienced relatively limited recent activity (Bufféral et al., 2023; Icelandic Met Office, 2023; Pedersen et al., 2023). In this context, numerical simulations of historical events such as the Veiðivötn 1477 CE eruption provide valuable insights into the potential impacts of large explosive eruptions on present-day populations, infrastructure, and air traffic under a range of atmospheric conditions. This is particularly relevant for long-term volcanic hazard assessment, as reflected in international initiatives led by the Icelandic government and the International Civil Aviation Organization (ICAO) between 2013 and 2016, which emphasize the need to consider both frequent moderate eruptions and rarer, larger-magnitude events (Barsotti et al., 2018).

4.2 **Limitations and future perspectives**

This study builds on the combination between field observations and numerical simulations to assess the potential of modelling tools for anticipating the impacts of future volcanic eruptions. Historical eruptions provide valuable reference cases to evaluate the consequences that similar eruptions could have under present-day conditions. This approach relies on the assumption that, although volcanic systems may evolve, some aspects of their eruptive behaviour and characteristic eruption styles can be used as a basis for scenario development. We investigate the worst case eruption scenario documented in Iceland during historical times, based on our current knowledge of the geological and historical records, without implying that a future eruption of similar magnitude is inevitable or ruling out the possibility of even larger events. The same methodology could also be applied to less extreme but potentially more frequent events that may nevertheless have significant impacts (e.g., the 2010 Eyjafjallajökull eruption). Given the large range of eruptive styles represented in Iceland,

458 applying this methodology to several volcanic systems would therefore be valuable. This could
459 ultimately lead to the development of a set of probabilistic hazard maps representing different
460 eruption scenarios, depending on the volcanic edifice involved and the areas potentially
461 exposed.

462 Applying this approach to volcanoes that are difficult to access, have sparse field data
463 or poorly documented eruptive histories could be more challenging. For volcanoes exhibiting
464 a large range of eruptive styles, obtaining reliable total grain-size distribution data and defining
465 potential impact zones would require investigating several eruptions, making the analysis
466 considerably more complex and time-consuming than for Veiðivötn. Furthermore, although
467 these maps provide valuable information for identifying potentially vulnerable areas, their
468 practical implications remain a challenge as evacuation or relocation can have significant
469 social and economic consequences for the local population (Benitez, 2018). The maps aim at
470 giving utils for local authorities to work with, in order to develop evacuation strategies that also
471 take into account the geographical and logistical constraints of the target territory, particularly
472 in island settings where evacuation options may be limited (Leone et al., 2019).

473 Another important aspect of this study is the seasonality of atmospheric circulation
474 over Iceland. We produced two seasonal probabilistic maps in order to represent the main
475 seasonal differences in tephra dispersal. However, April and August appear to be transitional
476 months (Figure 3) with more variable wind directions and speeds than during the main
477 seasonal periods. This variability makes tephra dispersal during these months more difficult
478 to assess using a simple seasonal classification. A useful extension of this work would be to
479 combine probabilistic hazard assessment with real-time meteorological forecasts when an
480 eruption is considered imminent. This approach would make it possible to account for actual
481 wind conditions expected at the time of the eruption, and thus provide more event-specific
482 forecasts of tephra dispersal. In such an unrest situation, however, the eruption source
483 parameters are unknown a priori, leading to significant uncertainties in hazard assessment.
484 Recent studies have investigated the possibility of constraining or retrieving these source

parameters in near real time during the early stages of an eruption using satellite observations (Michaud-Dubuy & Gouhier, 2025). Such approaches could therefore complement probabilistic modelling and progressively improve forecasts once an eruption has started.

5. - Conclusion

The Veiðivötn 1477 CE eruption provides a well-constrained case study to investigate the potential consequences of a large basaltic Plinian eruption under present-day atmospheric and societal conditions. We developed an integrated approach combining data measured in the field, numerical modeling of tephra dispersion, and the analysis of a 30-year meteorological database, in order to build probabilistic hazard maps. Our study shows that an event of this magnitude could produce impacts across a large range of spatial scales, from severe proximal fallout to atmospheric transport thousands of kilometers from Iceland.

We numerically reproduced the 1477 CE Veiðivötn eruption using the Fall3D model with an eruption duration of 12 hours and a maximum plume height of 30 km, constrained by the good agreement between observed and simulated tephra ground loads under realistic meteorological conditions. This supports the ability of the modelling approach to reproduce the main characteristics of the deposits pattern. We then performed Monte Carlo simulations to quantify the potential impacts of a future similar eruption. Depending on meteorological conditions, substantial tephra fallout could affect large parts of Iceland, with potentially significant consequences for transport networks, critical infrastructure, populated areas, agriculture, and economic activities. The 1,000 simulations performed with the 30-year meteorological dataset highlight the importance of wind speed and direction in controlling the spatial extent of tephra dispersal, these being governed by a marked seasonality throughout the year.Incorporating this variability is therefore essential for a realistic assessment of volcanic hazards.

The widespread atmospheric dispersal of the eruption is further supported by the occurrence of cryptotephra attributed to the Veiðivötn eruption in Greenland, Ireland, and

Sweden. These distal observations demonstrate that fine ash from a large basaltic Plinian eruption in Iceland can be transported over several thousand kilometers, with implications for aviation across the North Atlantic. Our approach supports long-term volcanic hazard assessment in Iceland by improving the understanding of rare, high-impact explosive scenarios and their potential consequences for present-day environments and society.

Acknowledgments

We are grateful to Á. Höskuldsson and T. Thordarson for initiating the research project on the 1477 CE Veiðivötn eruption and for providing financial support for M. Payet--Clerc. We thank W. M. Moreland and A. Michaud-Dubuy for fruitful discussions and helpful insights, and S. Bufféral for his critical comments on the manuscript.

References

Abbott, P. M., Plunkett, G., Corona, C., Chellman, N. J., McConnell, J. R., Pilcher, J. R., ... & Sigl, M. (2021). Cryptotephra from the Icelandic Veiðivötn 1477 CE eruption in a Greenland ice core: confirming the dating of volcanic events in the 1450s CE and assessing the eruption's climatic impact. *Climate of the Past*, *17*(2), 565-585.

Barsotti, S., Andronico, D., Neri, A., Del Carlo, P., Baxter, P. J., Aspinall, W. P., & Hincks, T. (2010). Quantitative assessment of volcanic ash hazards for health and infrastructure at Mt. Etna (Italy) by numerical simulation. *J. Volcanol. Geotherm. Res.*, *192*(1-2), 85-96.

Barsotti, S., Di Rienzo, D. I., Thordarson, T., Björnsson, B. B., & Karlsdóttir, S. (2018). Assessing impact to infrastructures due to tephra fallout from Öræfajökull volcano (Iceland) by using a scenario-based approach and a numerical model. *Frontiers in Earth Science*, *6*, 196.

533 Bénitez, F. (2018). *Faire face ou vivre avec les catastrophes? Capacités d'adaptation et*
534 *capabilités dans les trajectoires de résilience individuelles et territoriales au sein de*
535 *l'espace Caraïbe* (Doctoral dissertation, Université Paul Valéry-Montpellier III).

536 Benjamínsson, J., 1982. Gjóskulag á Norðausturlandi. Inn: Eldur er í Norðri (editors:
537 Helga Þórarinsdóttir, Ólafur H. Óskarsson, Sigurður Steinþórsson and Þorleifur
538 Einarsson). Reykjavík, Sögufélag, 181–185.

539 Biass, S., Scaini, C., Bonadonna, C., Folch, A., Smith, K., & Höskuldsson, A. (2014). A
540 multi-scale risk assessment for tephra fallout and airborne concentration from multiple
541 Icelandic volcanoes–Part 1: Hazard assessment. *Natural hazards and earth system*
542 *sciences*, *14*(8), 2265-2287.

543 Bonadonna, C., Connor, C. B., Houghton, B. F., Connor, L., Byrne, M., Laing, A., &
544 Hincks, T. K. (2005). Probabilistic modeling of tephra dispersal: Hazard assessment of a
545 multiphase rhyolitic eruption at Tarawera, New Zealand. *J. Geophys. Res. Solid Earth*,
546 *110*(B3).

547 Bonadonna, C., Pistolesi, M., Cioni, R., Degruyter, W., Elissondo, M., & Baumann, V.
548 (2015). Dynamics of wind-affected volcanic plumes: The example of the 2011 Cordón
549 Caulle eruption, Chile. *J. Geophys. Res. Solid Earth*, *120*(4), 2242-2261.

550 Bonasia, R., Capra, L., Costa, A., Macedonio, G., & Saucedo, R. (2011). Tephra fallout
551 hazard assessment for a Plinian eruption scenario at Volcán de Colima (Mexico). *J.*
552 *Volcanol. Geotherm. Res.*, *203*(1-2), 12-22.

553 Bonasia, R., Scaini, C., Capra, L., Nathenson, M., Siebe, C., Arana-Salinas, L., & Folch,
554 A. (2014). Long-range hazard assessment of volcanic ash dispersal for a Plinian eruptive
555 scenario at Popocatépetl volcano (Mexico): implications for civil aviation safety. *Bull.*
556 *Volcanol.*, *76*(1), 789.

557 Bufféral, S., Panza, E., Mannini, S., Hjartardóttir, Á. R., Nobile, A., Gies, N., ... & Ruch, J.
558 (2023). Surface fractures generated during the 2021 Reykjanes oblique rifting event (SW
559 Iceland). *Bulletin of Volcanology*, *85*(11), 64.

560 Carey, S., & Sigurdsson, H. (1987). Temporal variations in column height and magma
561 discharge rate during the 79 AD eruption of Vesuvius. *Geological Society of America*
562 *Bulletin*, *99*(2), 303-314.

563 Carey, S., Sigurdsson, H., Gardner, J. E., & Criswell, W. (1990). Variations in column
564 height and magma discharge during the May 18, 1980 eruption of Mount St. Helens. *J.*
565 *Volcanol. Geotherm. Res.*, *43*(1-4), 99-112.

566 Carlsen, H. K., Hauksdottir, A., Valdimarsdottir, U. A., Gíslason, T., Einarsdottir, G.,
567 Runolfsson, H., ... & Pétursdóttir, G. (2012). Health effects following the Eyjafjallajökull
568 volcanic eruption: a cohort study. *BMJ open*, *2*(6), e001851.

569 Chambers, F. M., Daniell, J. R., Hunt, J. B., Molloy, K., & O'Connell, M. (2004).
570 Tephrostratigraphy of An Loch Mor, Inis Oirr, western Ireland: implications for Holocene
571 tephrochronology in the northeastern Atlantic region. *The Holocene*, *14*(5), 703-720.

572 Chang, J. C., & Hanna, S. R. (2004). Air quality model performance evaluation.
573 *Meteorology and Atmospheric Physics*, *87*(1), 167-196.

574 Cioni, R., Longo, A., Macedonio, G., Santacroce, R., Sbrana, A., Sulpizio, R., &
575 Andronico, D. (2003). Assessing pyroclastic fall hazard through field data and numerical
576 simulations: example from Vesuvius. *J. Geophys. Res. Solid Earth*, *108*(B2).

577 Costa, A., Dell'Erba, F., Di Vito, M. A., Isaia, R., Macedonio, G., Orsi, G., & Pfeiffer, T.
578 (2009). Tephra fallout hazard assessment at the Campi Flegrei caldera (Italy). *Bulletin of*
579 *Volcanology*, *71*(3), 259-273.

580 Costa, A., Macedonio, G., & Folch, A. (2006). A three-dimensional Eulerian model for
581 transport and deposition of volcanic ashes. *Earth and Planetary Science Letters*, *241*(3-
582 4), 634-647.

583 Davies, S. M., Elmquist, M., Bergman, J., Wohlfarth, B., & Hammarlund, D. (2007).
584 Cryptotephra sedimentation processes within two lacustrine sequences from west central
585 Sweden. *The Holocene*, *17*(3), 319-330.

586 Deligne, N. I., Fitzgerald, R. H., Blake, D. M., Davies, A. J., Hayes, J. L., Stewart, C., ... &
587 Woods, R. (2017). Investigating the consequences of urban volcanism using a scenario
588 approach I: Development and application of a hypothetical eruption in the Auckland
589 Volcanic Field, New Zealand. *Journal of Volcanology and Geothermal Research*, *336*,
590 192-208.

591 Folch, A. (2012). A review of tephra transport and dispersal models: Evolution, current
592 status, and future perspectives. *J. Volcanol. Geotherm. Res.*, *235*, 96-115.

593 Folch, A., Costa, A., & Macedonio, G. (2009). FALL3D: A computational model for
594 transport and deposition of volcanic ash. *Computers & Geosciences*, *35*(6), 1334-1342.

595 Folch, A., & Sulpizio, R. (2010). Evaluating long-range volcanic ash hazard using
596 supercomputing facilities: application to Somma-Vesuvius (Italy), and consequences for
597 civil aviation over the Central Mediterranean Area. *Bull. Volcanol.*, *72*(9), 1039-1059.

598 Gonnermann, H. M., & Manga, M. (2007). The fluid mechanics inside a volcano. Annu.
599 Rev. Fluid Mech., 39(1), 321-356.

600 Gudmundsson, M. T., Pedersen, R., Vogfjörd, K., Thorbjarnardóttir, B., Jakobsdóttir, S., &
601 Roberts, M. J. (2010). Eruptions of Eyjafjallajökull volcano, iceland.

602 Holasek, R. E., Self, S., & Woods, A. W. (1996). Satellite observations and interpretation
603 of the 1991 Mount Pinatubo eruption plumes. *J. Geophys. Res. Solid Earth*, *101*(B12),
604 27635-27655.

605 Hurst, T., & Smith, W. (2004). A Monte Carlo methodology for modelling ashfall hazards.
606 *J. Volcanol. Geotherm. Res.*, *138*(3-4), 393-403.

607 Jenkins, S. F., Wilson, T. M., Magill, C., Miller, V., Stewart, C., Blong, R., ... & Costa, A.
608 (2015). Volcanic ash fall hazard and risk. *Global volcanic hazards and risk*, 173-222.

609 Kaminski, E., & Jaupart, C. (1998). The size distribution of pyroclasts and the
610 fragmentation sequence in explosive volcanic eruptions. *Journal of Geophysical*
611 *Research: Solid Earth*, *103*(B12), 29759-29779.

612 Lacasse, C. (2001). Influence of climate variability on the atmospheric transport of
613 Icelandic tephra in the subpolar North Atlantic. *Global and Planetary Change*, *29*(1-2), 31-
614 55.

615 Larsen, G. (1984). Recent volcanic history of the Veiðivötn fissure swarm, southern
616 Iceland—an approach to volcanic risk assessment. *J. Volcanol. Geotherm. Res.*, *22*(1-2),
617 33-58.

618 Larsen G (2005) Explosive volcanism in Iceland: three examples of phreatomagmatic
619 basaltic eruptions on long volcanic fissures within the past 1200 years. In: Geophysical
620 Research Abstracts (Vol 7, No. 10158, p 2005).

621 Larsen, G., & Gudmundsson, M. T. (2014). Volcanic system: Bárðarbunga system.
622 *Catalogue of Icelandic Volcanoes*, 1-11.

623 Leone, F., Komorowski, J. C., Gherardi-Leone, M., & Lalubie, G. (2019). Integrating
624 spatial accessibility in the design of volcano evacuation plans in the French West Indies
625 (Guadeloupe and Martinique). *Journal of Applied Volcanology*, *8*(1), 8.

626 Loughlin, S., Barsotti, S., Bonadonna, C., & Calder, E. (2017). 3.2 Geophysical risks:
627 volcanic activity. *Science for disaster risk management*, 151-190.

628 Macedonio, G., Costa, A., & Folch, A. (2008). Ash fallout scenarios at Vesuvius:
629 numerical simulations and implications for hazard assessment. *J. Volcanol. Geotherm.*
630 *Res.*, *178*(3), 366-377.

631 Michaud-Dubuy, A., Carazzo, G., & Kaminski, E. (2021). Volcanic hazard assessment for
632 tephra fallout in Martinique. *Journal of Applied Volcanology*, *10*(1), 8.

633 Michaud-Dubuy, A., Komorowski, J. C., Lacombe, T., & Gurioli, L. (2024). Tephra fallout
634 hazard assessment for a hydrovolcanic eruptive scenario in Mayotte. *Scientific Reports*,
635 *14*(1), 31880.

636 Michaud-Dubuy, A., & Gouhier, M. (2025). Validation of near real-time retrieval of plume
637 mass eruption rates: The case of the 2021 eruption of La Soufrière, St Vincent.
638 *Geochemistry, Geophysics, Geosystems*, *26*(10), e2025GC012498.

639 Michaud-Dubuy, A., Komorowski, J. C., & Carazzo, G. (2025). Tephra fallout and
640 dispersal modeling of phreatic eruptions: implications for volcanic hazard assessment in
641 Martinique and Guadeloupe (Lesser Antilles). *Bull. Volcanol.*, *87*(2), 11.

642 Moreland WM, Thordarson T, Houghton BF, Larsen G (2019) Driving mechanisms of
643 subaerial and subglacial explosive episodes during the 10th century Eldgjá fissure
644 eruption, southern Iceland. Volcanica 2(2):129−150. https:// doi. org/ 10. 30909/ vol. 02.
645 02. 129150

646 Moriasi, D. N., Arnold, J. G., Van Liew, M. W., Bingner, R. L., Harmel, R. D., & Veith, T. L.
647 (2007). Model evaluation guidelines for systematic quantification of accuracy in watershed
648 simulations. *Transactions of the ASABE*, *50*(3), 885-900.

649 Payet, M. (2026) New insights on the dynamics of Plinian basaltic eruptions: Field
650 reconstruction and physical modeling of the Veiðivötn 1477 CE basaltic eruptive plume,
651 PhD thesis, Université Paris Cité & University of Iceland, 324 p.

652 Payet--Clerc, M., Carazzo, G., Moreland, W. M., Thordarson, T., Valdimarsdóttir, I. K., &
653 Höskuldsson, Á. (2026). The Veiðivötn 1477 CE basaltic Plinian eruption: retrieving
654 source parameters through field work and 1D physical plume modelling. *Bull. Volcanol.*,
655 *88*(5), 52.

656 Pedersen, G. B., Pfeffer, M. A., Barsotti, S., Tarquini, S., de'Michieli Vitturi, M., Óladóttir,
657 B., & Þrasstarson, R. H. (2022). Lava flow hazard modelling during the 2021
658 Fagradalsfjall eruption, Iceland: Applications of MrLavaLoba. *Natural Hazards and Earth*
659 *System Sciences Discussions*, *2022*, 1-38.

660 Scaini, C., Folch, A., & Navarro, M. (2012). Tephra hazard assessment at Concepción
661 volcano, Nicaragua. *J. Volcanol. Geotherm. Res.*, *219*, 41-51.

662 Scaini, C., Biass, S., Galderisi, A., Bonadonna, C., Folch, A., Smith, K., & Höskuldsson,
663 A. (2014). A multi-scale risk assessment for tephra fallout and airborne concentration
664 from multiple Icelandic volcanoes–Part 2: Vulnerability and impact. *Natural Hazards and*
665 *Earth System Sciences*, *14*(8), 2289-2312.

666 Schyberg, H., Yang, X., Køltzow, M., Amstrup, B., Bakketun, Å., Bazile, E., ... & Wang, Z.
667 (2020). Arctic regional reanalysis on single levels from 1991 to present. *Copernicus*
668 *Climate Change Service (C3S) Climate Data Store (CDS)*, *10*.

669 Scollo, S., Coltelli, M., Bonadonna, C., & Del Carlo, P. (2013). Tephra hazard assessment
670 at Mt. Etna (Italy). *Natural Hazards and Earth System Sciences*, *13*(12), 3221-3233.

Spence, R. J. S., Kelman, P. J., Zuccaro, G., Petrazzuoli, S., Baxter, P. J., Marti, J., & Felpeto, A. (2005). Residential building and occupant vulnerability to tephra fall. *Natural Hazards & Earth System Sciences*, *5*(4).

Thordarson, T., & Höskuldsson, Á. (2008). Postglacial volcanism in Iceland. *Jökull*, *58*(198), e228.

Thorvaldsdóttir, S., & Sigbjörnsson, R. (2015). Framing the 2010 Eyjafjallajökull volcanic eruption from a farming-disaster perspective. *Natural Hazards*, *77*(3), 1619-1653.

Walker, G. P. (1980). The Taupo pumice: product of the most powerful known (ultraplinian) eruption?. *J. Volcanol. Geotherm. Res.*, *8*(1), 69-94.

Watt, S. F., Pyle, D. M., Mather, T. A., Martin, R. S., & Matthews, N. E. (2009). Fallout and distribution of volcanic ash over Argentina following the May 2008 explosive eruption of Chaitén, Chile. *J. Geophys. Res. Solid Earth*, *114*(B4).

Wilson, T. M., Stewart, C., Sword-Daniels, V., Leonard, G. S., Johnston, D. M., Cole, J. W., ... & Barnard, S. T. (2012). Volcanic ash impacts on critical infrastructure. *Physics and Chemistry of the Earth, Parts a/b/c*, *45*, 5-23.

Wohletz K, Zimanowski B, Büttner R (2013) Magma-water interactions. In: Modeling volcanic processes: the physics and mathematics of volcanism, pp 230–257.

Statements and Declarations

Funding This work was funded by i) TelluS of the Institut National des Sciences de l'Univers, CNRS, ii) the Jules Verne 2024 programme funded by the French Ministry for Europe and Foreign Affairs and the French Ministry for Higher Education and Research, iii) the Icelandic Research Fund, from the Icelandic Center for Research (Rannis), grant number: 239876-051. This study contributes to the Idex project "Université Paris Cité" (ANR-18-IDEX-0001).

Competing Interests The authors have no relevant financial or non-financial interests to disclose.

Author Contribution

Léa Guichard developed the methodology in collaboration with **Guillaume Carazzo**, carried out the numerical simulations, performed the probabilistic analyses, produced the hazard maps, interpreted the results, and prepared the first draft of the manuscript. **Méline Payet--Clerc** conducted fieldwork and provided the field measurements of tephra ground load used for model evaluation. **Guillaume Carazzo** conceived and supervised the project, contributed to the development of the methodology and interpretation of the results. **Laurie Barrier** contributed to the methodology and wind data analysis by providing analysis scripts and through scientific discussions. All authors contributed to the discussion of the results, reviewed the manuscript, and approved the final version.

Supplementary Files

This is a list of supplementary files associated with this preprint. Click to download.

- SI.pdf